Acoustic Propagation in an Arctic Shallow-Water Environment

[1]FRANCINE DESHARNAIS, [1]GARRY J. HEARD, [1]GORDON R. EBBESON, [1]DAVID J. THOMSON,
[2]DOUGLAS J. SCHILLINGER, [1]RAJVEER SEYAN
[1]DEFENCE RESEARCH & DEVELOPMENT CANADA – ATLANTIC
9 GROVE STREET, PO BOX 1012, DARTMOUTH, NOVA SCOTIA, CANADA, B2Y 3Z7
[2]GALE FORCE SCIENTIFIC CONSULTING LTD
81 NEWCASTLE ST, DARTMOUTH, NOVA SCOTIA, CANADA, B2Y 3M8

***Abstract*- A short-range, shallow-water transmission loss experiment was conducted in the South Lincoln Sea, under an irregular rough ice canopy. A barrel-stave source was used to transmit 800-Hz tonal signals at depths of 10 and 30 m. The signals were received on a four-element vertical line array distributed over the 65-m water depth. To support the transmission loss measurements, a bottom loss experiment was carried out using broadband signals generated by imploding light bulbs at three depths and with data received on the same hydrophone array. Previous drilling experiments in the vicinity of this site have provided seabed information and revealed the presence of a subbottom permafrost layer. Preliminary modeling of the acoustic propagation in this highly irregular channel was carried out using a wave-based model. This paper reviews the measurements, and discusses the challenges associated with the modeling, in view of the experimental uncertainties associated with this complicated environment.**

I. INTRODUCTION

The Lincoln Sea covers a large area in the Arctic bounded by Ellesmere Island to the south, Greenland to the east and by approximately the 84th parallel. The margin of the sea is the continental shelf extending 200 km to the north of Ellesmere Island, a shelf break and a deep basin. Limited information is available on the geo-acoustic properties of the shallow-water area near the coast, mainly due to the difficulties associated with seismic or geo-acoustic experiments in this isolated area.

A trial was conducted on shore-fast ice west of CFS Alert, on the north coast of Ellesmere Island, in March-May 2002. The ice camp location is shown in Fig. 1. Using the ice as a platform, a bottom loss experiment was carried out using broadband signals generated by imploding light bulbs. A short-range, shallow-water transmission loss experiment was conducted with tonal signals transmitted with a barrel-stave source.

This paper reviews some of the geo-acoustic information available for the area. The results from the bottom loss and transmission loss experiments are presented and put in context of the wider body of information available.

II. THE SOUTH LINCOLN SEA

A wide-scoped environmental report by Bucca [1] describes the circulation, water masses, surface ice condition and bottom types of the Lincoln Sea. The oceanography is driven by the Arctic Surface Water, a cold (< 0°C) and fresh (< 34.5 PSU) water mass. At depths from less than 30 to 50 m, the layer is well mixed. The sound speed profile of the surface layer has a small positive gradient. The details of the surface water vary spatially within the Arctic Basin.

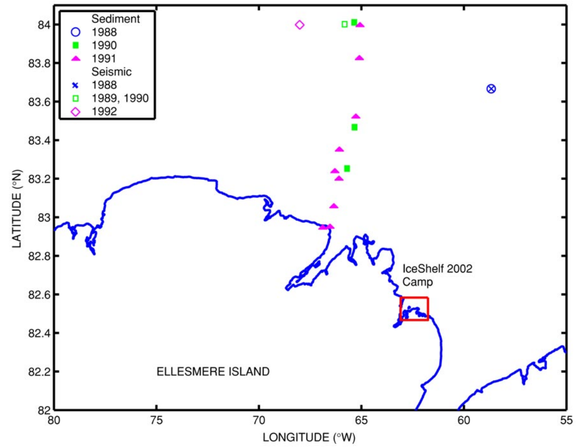

Fig. 1. Iceshelf 2002 camp location (box), core sample site from 1988 (circle), sediment sample sites from 1990 (filled squares) and 1991 (triangles) and seismic experiment locations from 1988 (cross), 1989 (hollow square) and 1992 (diamond).

Sediment in the area is transported from Greenland and Ellesmere Island via ice and consists of clay and silt, as well as coarse sediment ranging from gravel to boulder size. A core sample was taken in 1988 [2], 80 nm north of Alert, and sediment samples were taken in 1990 and 1991 along a transect from Stuckberry point north into the Lincoln Sea (Fig. 1). Analysis of the core sample from 1988 [2] gives a bulk density (ρ) of 2.14 g cm^{-3}, a porosity of 40.7% and a compressional sound speed (c_p) of 1794 m s^{-1} at the surface of the bottom layer.

Sediment size distribution from the four locations nearest the coast taken in 1991 [1] have gravel content and clay content that vary from 0.2% to 46% and 27% to 71% respectively. Results from all locations show that the surface layer varies considerably but is mainly composed of silt and clay with varying amounts of gravel with no discernable trend in grain size variability.

Seismic measurements collected in 1988 [3], 1989 [1], 1990 [4], 1992 [5] were all collected near the shelf break in deep water (> 400 m), north of Ellesmere Island (see Fig. 1). The results from 1988 showed velocities at the surface of the bottom layer of 1980 m s^{-1}.

Hunter [6] showed three principle layers at the 1989 site, where the depth of the top layer varied significantly with range from the source. At this location, the c_p was estimated at 1820 m s^{-1}. His analysis of the data from 1990 showed a surface bottom layer with velocity ranging from 1750 to 2000 m s^{-1}.

Dosso's analysis [5] of seismic data from 1992 shows that a lower velocity surface layer is present with a c_p of 1720 ± 100 m s^{-1} and a thickness (h) of 10 ± 4 m. The layer below that had a c_p of 1900 ± 10 m s^{-1}.

Geddes [7] made a geo-acoustic model using classical theory of the origin of the continental shelves in the Arctic. This model was updated using the seismic measurements from 1989 and the 1988 core sample. He calculated a reflection coefficient of 0.5, or a bottom loss of 6.0 dB, given a bottom water velocity of 1505 m s^{-1} and a bottom layer velocity of 1738 m s^{-1}.

The results from these studies are summarized in Table 1.

TABLE I. SUMMARY OF GEO-ACOUSTIC PARAMETERS – SEABED

Author	Year of data collection	Geo-acoustic Property	Experimental Value
Todoeschuk [4]	1988	c_p	1980 ± 10 m s^{-1}
Mayer and Marsters [2]	1988	c_p	1683 m s^{-1}
		ρ	2.14 g cm^{-3}
Geddes [7]	1988-89	R	0.5
		c_p	1738 m s^{-1}
Hunter and Pullan [6]	1989	c_p	1820 m s^{-1}
	1990	c_p	1710 – 2000 m s^{-1}
Dosso and Brooke [5]	1992	c_p (upper layer)	1720 ± 100 m s^{-1}
		h (upper layer)	10 ± 4 m
		c_p (lower layer)	1900 ± 10 m s^{-1}

Fig. 2 shows a diagram of a geological model for Jolliffe Bay, where the ice camp was located. This diagram is a composite view based on [8], and physical observations from 2002. The horizontal scale of this figure is 3 km; the 2002 ice camp would be on the left, at 65-m water depth.

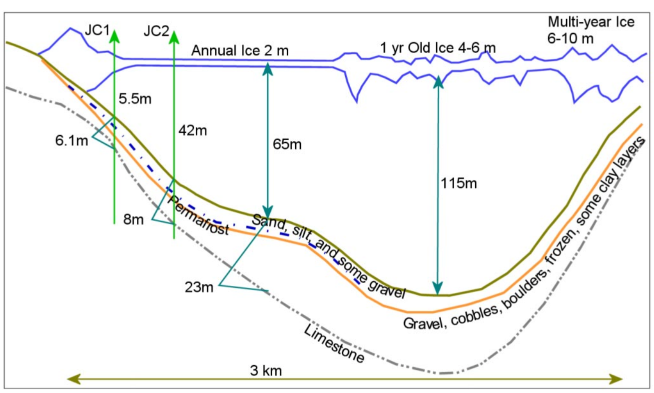

Fig. 2. Geo-physical model of Jolliffe Bay, along a SW-NE transect.

The upper sediment is a thin layer of sand and/or silt, varying in thickness to an estimated ~7 m in the deepest part of the bay. This silt layer is frozen at depths greater than 1.5 m at JC1 (drill hole) and at depths greater than 5.5 m at JC2. The frozen region appears to extend to the bedrock, and contains lenses of unfrozen material. A thin (~5-m thick) layer of a mix of gravel and cobbles of varying sizes overlays the bedrock (argillaceous limestone). This model is approximate, and extrapolates heavily from the limited data available for this area.

The ice cover in the area varied from annual ice at the camp to first-year and multi-year ice, as shown. In the north-eastern side of the bay (right-hand side of the figure), the ice was generally older and thicker.

The ice cover can influence acoustic propagation, especially at long range. Table II includes geo-acoustic properties of sea ice, as reviewed by Dosso, Heard and Vinnins [9].

TABLE II. SUMMARY OF GEO-ACOUSTIC PARAMETERS – ICE COVER

Author	Year of data collection	Geo-acoustic Property	Experimental Value
Miller and Schmidt [10], for 2.4-m ice	1987	c_s	1750 m s^{-1}
Brooke and Ozard [11], for smooth ice	1986	c_s	1891 m s^{-1}
		c_p	2960 m s^{-1}
	1987	c_s	1705 m s^{-1}
		c_p	3084 m s^{-1}
Yang and Giellis [12], for ~2-m ice	1988	c_s	1650 m s^{-1}
		c_p	2800 m s^{-1}

III. EXPERIMENTAL SETUP

Fig. 3 shows a close-up of the location of the camp in Jolliffe Bay, where the receiving array was located. It also shows the location of the source positions for the transmission loss experiment (filled circles). The bottom loss experiment was centred within 150 m of the array (not shown in this figure).

The receiving array was a Vertical Line Array (VLA) of four hydrophones at depths of 20, 30, 40 and 50 m. The array was fixed throughout the experiments, while sources were lowered through ice holes located at various ranges. Broadband signals generated by imploding light bulbs [14] were used for the bottom loss experiment, while 800-Hz tonal signals transmitted with an 800-Hz barrel-stave transducer were used for the transmission loss experiment.

The signals from the four hydrophones were digitized at a sampling rate of 2560 Hz and recorded on a battery-powered multi-channel data acquisition system.

A collection of temperature and sound-speed profiles recorded in April 2002 with a profiler from Applied Microsystems Ltd. are shown in Fig. 4. All profiles are consistent with the Arctic Surface Water described by Bucca [1]. The sound speed profile used for the data processing and modelling is shown as a thick line.

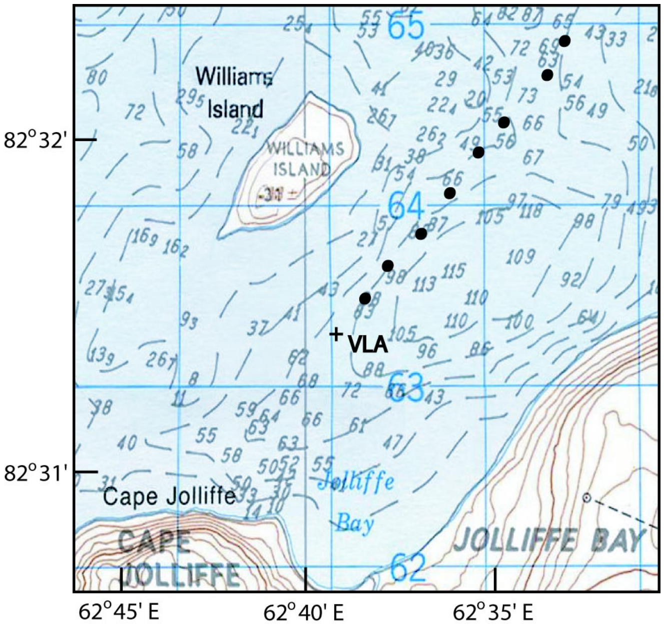

Fig. 3. Jolliffe Bay [13].

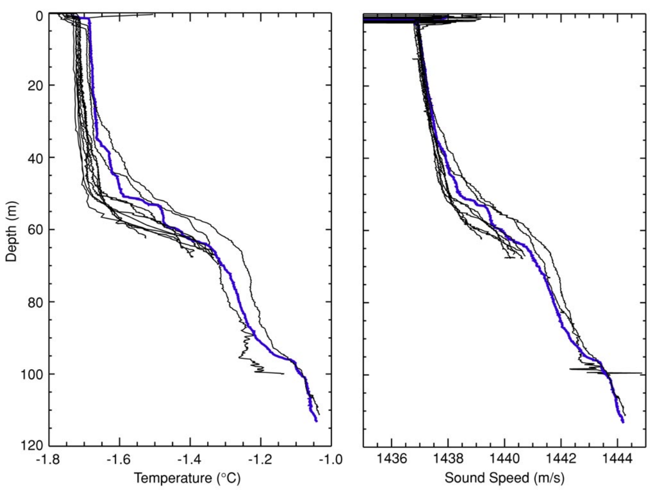

Fig. 4. Temperature and sound-speed profiles taken 12-24 April 2002. The profile shown as a solid thick line was used for the transmission loss processing.

A. Bottom loss processing

A light bulb breaking apparatus was used to control the depth of the implosion. Implosions from ten locations (bottom loss holes) at distances from 15 to 150 m from the VLA were recorded. At each location, the depth of the light-bulb breaker was set to 15, 30 and 50 m. At least three bulbs were used at each depth and location. The ranges between the sources and the receiving array were determined using a geodimeter, and are considered accurate within 20 cm.

Ray paths (lengths and grazing angles) were determined for each unique geometry using the ray model BELLHOP [15]. Bathymetry was included in the ray path analysis, where the depth is assumed to vary linearly between ice holes. Path lengths were converted to travel times using a mean sound speed in the water of 1438 m s^{-1}.

For each implosion the direct arrival was isolated by searching the output of each hydrophone for the peak voltage. The start and end of the light bulb signal was determined from visual inspection of the time series. From this method, the beginning of the signal from the light bulb implosion occurred 3.5 ms earlier than this peak. The end of the time series varies with the depth of the implosion, but on average is approximately 11.5 ms after the peak. The total length of the direct arrival light bulb signal is therefore 15 ms, which is consistent with Heard *et al.* [14].

Subsequent arrivals are detected by searching for maxima in the lagged cross-correlation function of the direct arrival signal and a portion of the recorded time series beginning 80 ms prior to the direct arrival and ending 100 ms after the direct arrival. Correlations less than 0.75 were discarded to avoid signal distortion by overlapping rays.

The predicted ray arrival times from BELLHOP are also used to exclude arrivals that overlap in time. If any ray arrived at a hydrophone within 7.5 ms (half the length of the light bulb signal) of the start of an earlier arrival, the earlier arrival was discarded from the analysis. If the earlier arrival was the direct ray, the entire record was discarded. A threshold of 7.5 ms allowed for some overlap in signals, but this was necessary to allow for detections from the bottom loss holes at greater distances from the receiver; only a small fraction of the light bulb signal energy is outside of the 7.5 ms window.

Once distinct arrivals were isolated they were then matched to the ray paths predicted using BELLHOP. Observed arrivals within ±5 ms of a predicted arrival were matched. If a measured ray matched more than one predicted ray using this method, the measured ray was matched to the predicted array whose arrival time was closest to the measured arrival time.

Spectral densities were calculated using a 64-point FFT (6 ms), a Hann window of width 16 points and 50% overlap (zero padded), resulting in 33 frequency bands and a spectral resolution of 39 Hz. The time series of the bulb implosion are 15 ms long, allowing four windows to be averaged. For each hydrophone and each light bulb implosion, the spectral energy of background noise was calculated using one second of the recorded time series starting two seconds before the direct arrival, and the same parameters as those for the signal spectral levels. The spectral noise levels were subtracted from the received spectral levels.

To correct for the spreading losses of the direct ray, the path lengths determined via BELLHOP were used. For the bottom-reflected rays, the difference in the arrival time of the direct and reflected ray was used to estimate the difference in path length between these two rays. The total path length of each bottom-reflected ray is the sum of the direct path plus the path length difference. This estimate of path length was used instead of the path length of the predicted bottom-reflected ray from BELLHOP since matched rays were sometimes mis-timed by as much as 5 ms.

To better estimate grazing angle, the angle the ray segment made with the horizontal minus the angle given by the interpolated bathymetry at the reflection point was used to obtain the actual grazing angle at the seabed interface. Only rays interacting with the bottom were kept; surface reflected paths were ignored due to the uncertainty associated with the rough ice surface.

B. *Transmission loss processing*

The same receiving array was employed for this experiment as for the bottom loss experiment. A barrel-stave transducer was used to transmit 45-s long tones centred at 800 Hz at 10- and 30-m depths. Fig. 5 shows a schematic of the experimental setup. The range scale on the lower part of the diagram indicates the ranges of the ice holes through which the source was lowered. These ranges were estimated from GPS positions.

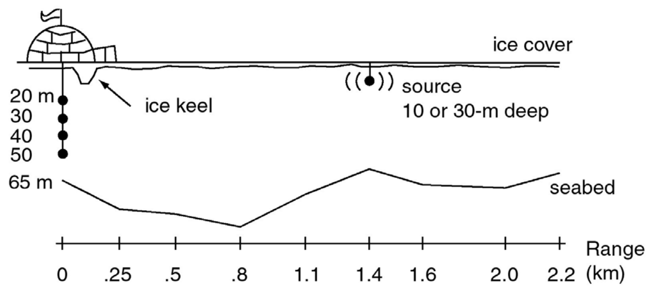

Fig. 5. Setup of the transmission loss experiment.

The water depth was measured at each ice hole, and linearly interpolated between holes. The ice thickness was also measured at each hole, and varied between 1.8 and 2.2 m in thickness. It should be noted that thin ice locations were purposely sought to simplify the drilling procedure. In general, most of the propagation was under first-year ice, except at the 2.0 and 2.2 km ranges where it was under multi-year ice. The precise thickness of the ice is unknown over the propagation paths, however, an ice keel estimated to be 10 to 15 m in depth was located between the receiver, and the first source hole 250 m away.

A 36-s long data segment from each received signal was selected and processed with 2560-pt FFTs overlapped by 50%. A Hann window was used. The averaged levels were calibrated and corrected for the appropriate gains.

IV. BOTTOM LOSS

A. *Measurements*

Fig. 6 shows the bottom loss data as a function of grazing angle at the three frequencies of 120, 520 and 800 Hz (star symbols). These data are based on rays that interact only with the seabed, with no surface reflections.

There is a significant amount of scatter in the data, but a critical angle of approximately 30-35° can be seen in the data. This angle corresponds to a sound speed in the seabed on the order of 1700 m s^{-1}. The structure of the bottom loss data in Fig. 6 suggests that the surficial sediment is layered.

The low bottom losses at 75° are probably due to the transmission loss (taken as spherical spreading) being overestimated along each path. This effect would be more important at short range – or high grazing angles – where path length differences are higher.

The bottom loss levels agree with the seabed reflection coefficient of 0.5 dB (or bottom loss of 6 dB) of Geddes [7].

B. *Modelling*

The bottom loss data were modelled from the reflection coefficient of a multi-layered fluid-solid structure, following the treatment of Jensen *et al*. [16]. We limited the model to a single fluid layer on top of a solid half-space.

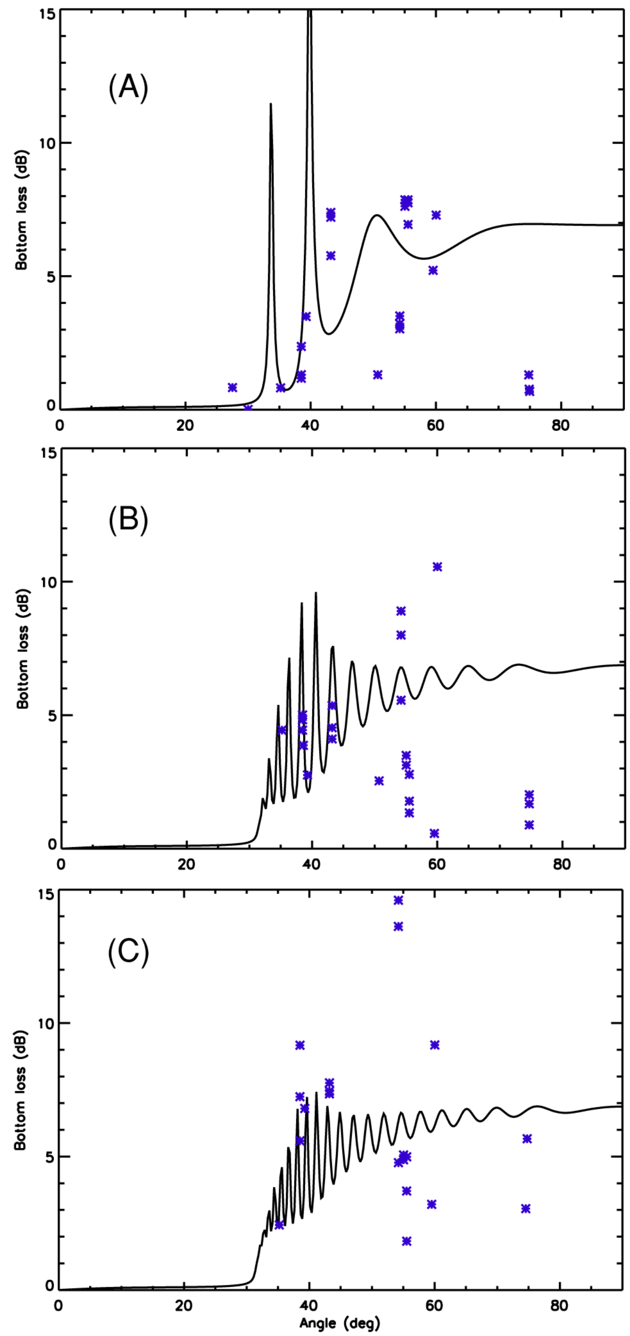

Fig. 6. Bottom loss for one-bottom-reflection rays plotted against grazing angle (degrees) for (A) 120 Hz; (B) 520 Hz; and (C) 800 Hz. Star symbols: data; solid line: model.

Since the data were available over a broad range of frequencies, an inversion technique was used to estimate geo-acoustic properties from the data. To search the space efficiently we use the hybrid Simplex Simulated Annealing (SSA) search technique originally developed by Press *et al.* [17], and adapted to geo-acoustic inversion problems by Dosso *et al*. [18]. SSA combines the strengths of the Down Hill Simplex (DHS) method for minimizing a function locally, and Simulated Annealing (SA) that is effective for global minimization.

The cost function used in the inversion algorithm is the RMS difference between the modeled and measured bottom loss (dB) as a function of grazing angle θ:

$$E(\mathbf{m}) = \sum_{f=1}^{F}\left[\sum_{i}(\mathrm{BL}_{f}(\theta_i) - \mathrm{BL}'_{f}(\mathbf{m},\theta_i))^2\right]^{1/2}, \qquad (1)$$

where $\mathrm{BL}_f(\theta_i)$ is the measured bottom loss at a frequency f, and $\mathrm{BL'}_f(\mathbf{m},\theta_i)$ is the replica bottom loss computed for model parameters $\mathbf{m}=\{m_j, \quad j=1,\ldots,M\}$. The cost function is accumulated over F available frequencies.

The geo-acoustic parameters to be estimated are the compressional speed and attenuation, density, and thickness of the surficial layer and underlying half-space, and the shear speed and attenuation of the half-space (*i.e.,* $\mathbf{m}=\{c_{p1}, \alpha_{p1}, \rho_1, h_1, c_{p2}, c_{s2}, \alpha_{p2}, \rho_2, \alpha_{s2}\}$).

Fifteen 40-Hz bands regularly spaced from 40 to 1240 Hz were selected for the inversion. The bottom loss data for the grazing angle of 75° were not used in the inversion. The results for the main parameters are shown in Table III. The modelled bottom loss based on these parameters are shown in Fig. 6 (solid lines).

TABLE III. INVERTED GEO-ACOUSTIC PARAMETERS

Parameter	Estimate from inversion
α_{p1}	1683 m s^{-1}
ρ_1	2.3 g cm^{-3}
h_1	23.6 m
c_{p2}	1909 m s^{-1}
c_{s2}	100 m s^{-1}
ρ_2	2.0 g cm^{-3}

The inverted results for compressional sound speed (both layers) and sediment thickness are similar to those of Dosso [5] listed in Table I. The density of the surficial layer is higher than expected for the given values of compressional sound speed, mainly due to the large scatter in the bottom loss data at high frequency. The shear speed of the half-space reached the lower inversion limit set for the parameter; a change to a more realistic value of 350 m s^{-1} increased the cost function only by a small percentage, confirming that the compressional sound speed of the half-space had a low impact on the bottom loss over such a thick sediment layer.

V. TRANSMISSION LOSS

A. Measurements

Fig. 7 shows the measured transmission loss (diamond symbols) as a function of depth for the four receivers and seven source-receiver ranges. The 800-Hz source was at 10-m depth.

B. Modelling

Transmission loss as a function of depth was modelled using the range-dependent, parabolic equation model PECan [19]. Because of the varying bathymetry, the propagation was modelled from each source back towards the receiving array. The geo-acoustic parameters inverted from the bottom loss data (previous section) were used for the transmission loss modelling.

The results overlay the data in Fig. 7 (solid lines). The agreement between the data and the modelled results is generally good; the ~10 dB scatter in the data is reflected by a similar scatter in the model results. The depth dependency of the levels is generally within this 10-dB scatter.

The full field model results are shown in Fig. 8 for four selected ranges: 0.5, 1.1, 1.6 and 2.2 km; the receiver is located at 0 km, and the 10-m source is at the listed ranges. At such short ranges, the bathymetry has only a small impact on the mean transmission loss; outside of local variabilities, the average levels are similar at a given range from the source independent of the location of the source or water depth at the source location.

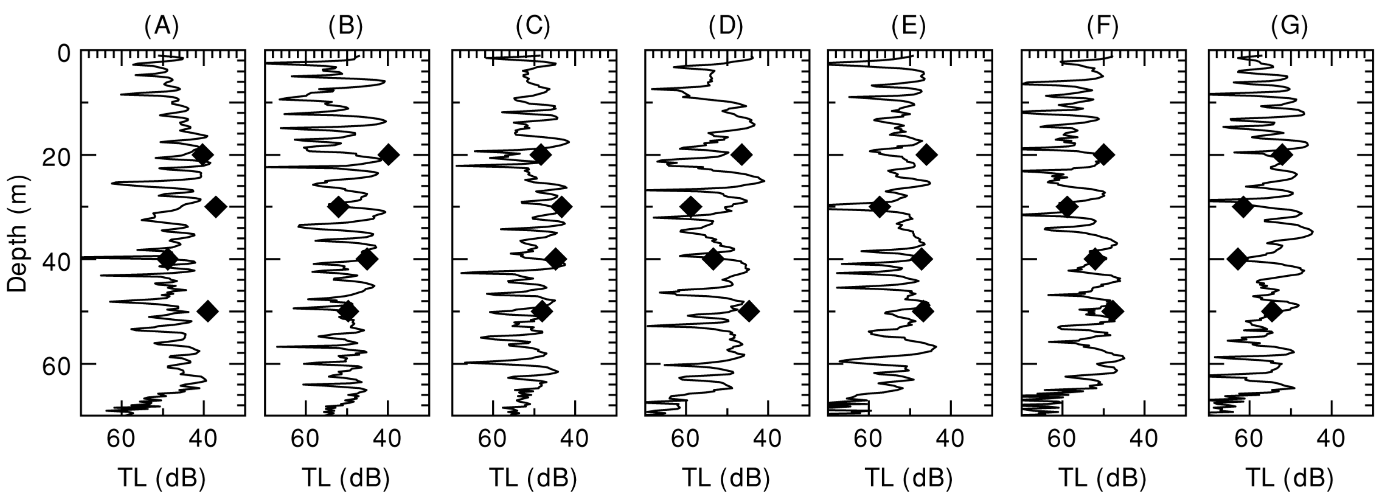

Fig. 7. Transmission loss as a function of depth at 800 Hz, for a 10-m deep source, for a receiver located at (A) .5 km; (B) .8 km; (C) 1.1 km; (D) 1.4 km; (E) 1.6 km; (F) 2 km and (G) 2.2 km. Diamonds: data; solid line: model.

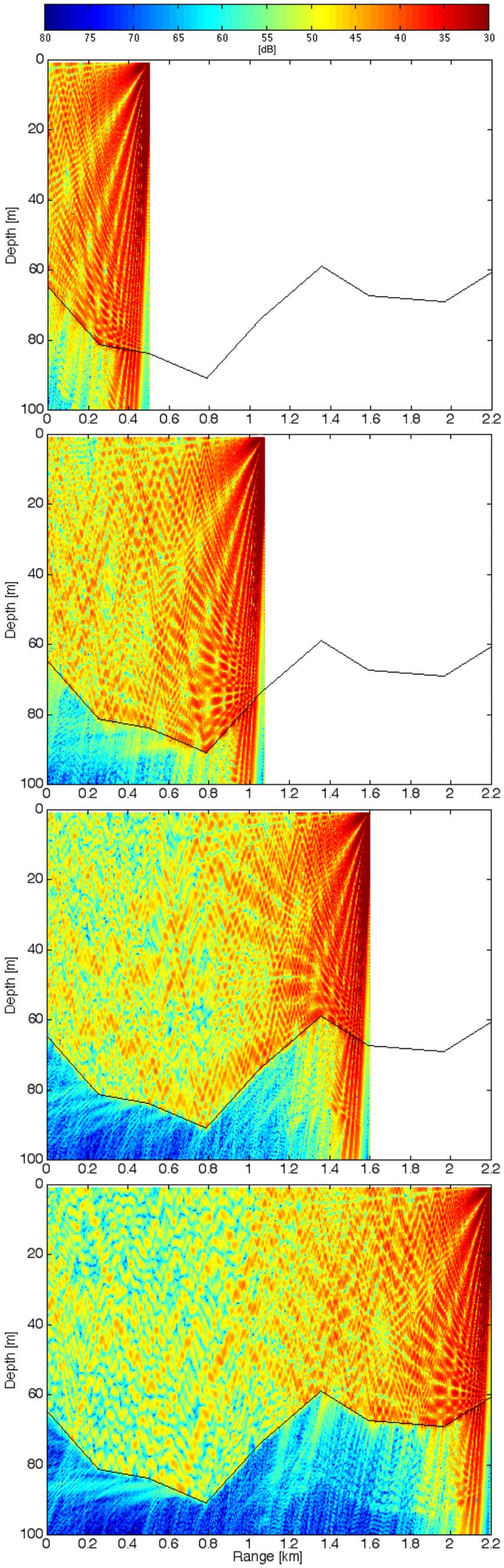

Fig. 8. Modelled transmission loss as a function of range and depth at 800 Hz, for a 10-m deep source located at .5 km (first panel); 1.1 km (second panel); 1.6 km (third panel); and 2.2 km (fourth panel).

The modelled results were averaged over a depth range of 20 to 50 m, for each source-receiver separation, for frequencies of 200, 400 and 800 Hz, and source depths of 10 and 30 m (Fig. 9). This figure demonstrates that transmission losses are expected to show little dependence over frequency for such short ranges.

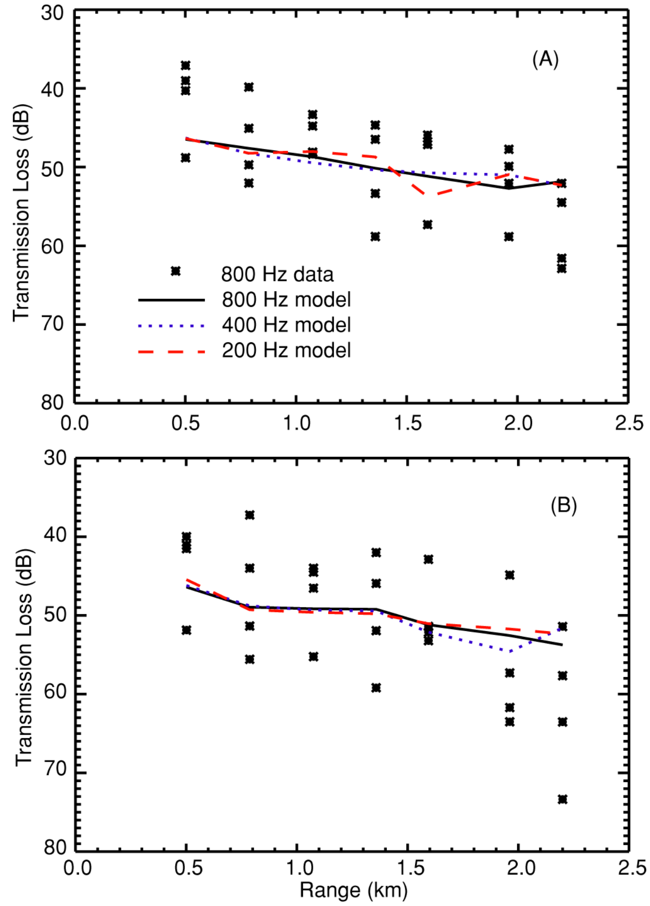

Fig. 9. 800-Hz data (star symbols) and depth-averaged modelled transmission loss at each range step for (A) 10-m deep source and (B) 30-m deep source at the frequency of 800 Hz (solid line), 400 Hz (dotted line) and 200 Hz (dashed line).

To verify the impact of the ice cover on transmission losses, the losses were modelled using the range-independent full-wave model SAFARI [20]. A compressional sound speed of 2800 m s^{-1}, compressional attenuation of 1.5 dB λ^{-1}, shear speed of 1700 m s^{-1}, shear attenuation of 0.9 dB λ^{-1}, and density of 0.9 g cm^{-3} were used for the simulations. To emphasize the differences, the transmission losses were computed to a range of 5 km, and the final curves were averaged with a moving-average window of 50 m in width for clarity. The results are shown in Fig. 10 for an 800-Hz source located at 10-m depth, and a receiver at 30-m depth; the ice cover is a smooth 2-m thick layer. The transmission loss with the ice cover (dotted line) is on the order of 5 dB higher than without the ice cover (solid line) at a range of 5 km. At ranges less than 2 km, the 2-3 dB difference is negligible. The effect of scattering from the rough ice cover was not included in the modeling since insufficient roughness information was available.

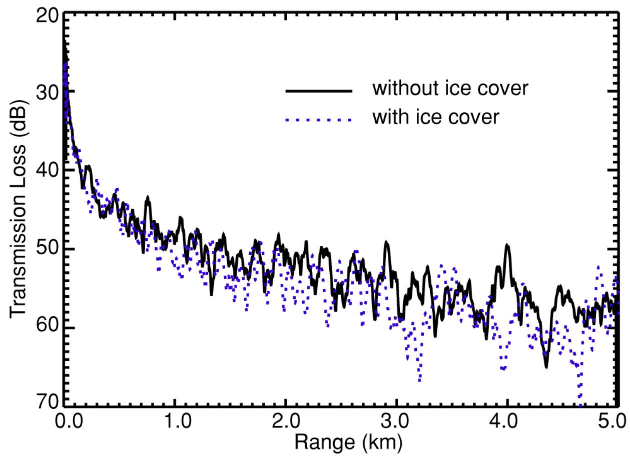

Fig. 10. Transmission loss as a function of range for a 10-m deep source and a 30-m deep receiver at the frequency of 800 Hz, without an ice cover (solid line), and with a 2-m thick ice cover (dotted line).

VI. SUMMARY

Gathering geo-acoustic data in an Arctic setting is difficult at the best of times, and this is reflected in the small amount of data available in the literature. This paper collects a significant amount of information about an Arctic environment.

A bottom loss and a transmission loss experiment were conducted in shallow water under an ice cover in April 2002. The ice cover greatly limited the amount of data that could be collected: only the single bottom-reflected paths from the bottom loss experiment could be used, and transmission loss data were limited to a few accessible ice holes.

The collected data agree with previously-published information for the area. Longer ranges would be required to fully determine the impact of the seabed on transmission loss. It was determined, however, that at short ranges transmission loss is relatively independent of the ice canopy and seabed structure.

ACKNOWLEDGMENTS

The data were collected by the dedicated Iceshelf 2002 team; their enthusiasm led to the remarkable average of 1.5 min per light bulb implosion, in challenging Arctic conditions.

The authors extend special thanks to Dr Stan Dosso, University of Victoria, for his suggestion of using light bulbs for the bottom loss experiment.

REFERENCES

[1] Bucca, P.J. A compendium of environmental data collected during the Iceshelf-99 exercise. Technical Note 32, Naval Oceanographic and Atmospheric Laboratory, Stennis Space Center, Mississippi, 1992.

[2] Mayer, L.A., and Marsters, J. Measurement of geophysical properties of arctic sediment cores. Contractors report series 89-19, Defence Research Establishment Pacific, Victoria. 1989.

[3] Nelson, J.B., Harwick, D., Bower, M., Marcotte, D. MacPherson, M., Forsythe, D., Macnab, R. and Teskey, D. Preliminary analysis of data from the Lincoln Sea aeromagnetic survey 1989-1990. Geological Survey of Canada Current Research, Ottawa. 1991.

[4] Todoeschuck, J.P. Seismic experiments in the Lincoln Sea during IceShelf 88. Contractors report 90-25, Defence Research Establishment Pacific, Victoria 1990.

[5] Dosso, S.E, Brooke, G.H. Measurements of seismo-acoustic ocean-bottom properties in the high Arctic. J. Acoustic. Soc. Am. 98(3), 1657-1666 (1995).

[6] Hunter, J.A., and Pullan, S.E. A vertical array method for shallow seismic refraction surveying of the sea floor. Geophysics, 55, 92-96 (1990).

[7] Geddes, W.H. Geoacoustic model Lincoln Sea. Geddes Geophysical Associates Technical Report 3-90, 23 pp., 1990.

[8] Forsyth, R.J., A.J. Hanna, D.S. Cayers, 1993 Iceshelf drilling program – geotechnical survey of prospective directional hole alignments, Dumbell Bay, Stuckberry East Bay and Jolliffe Bay, NWT, Defence Research Establishment Pacific Contractors Report 93-48, 1993.

[9] Dosso, S.E., G.J. Heard, M. Vinnins, Source bearing estimation in the Arctic Ocean using ice-mounted geophones, J. Acoustic. Soc. Am. 112(6), 2721-2734, 2002.

[10] Miller, B.E. and H. Schmidt, Observation and inversion of seismo-acoustic waves in a complex arctic ice environment, J. Acoust. Soc. Am. 89, 1668-1685, 1991.

[11] Brooke, G.H. and J.M. Ozard, In-situ measurement of elastic properties of sea ice, in Underwater Acoustic Data Processing, edited by Y.T. Chan, Kluwer Academic, Dordrecht, The Netherlands, pp. 113-118, 1989.

[12] Yang, T.C. and G.R. Giellis, Experimental characterization of elastic waves in a floating ice sheet, J. Acoust. Soc. Am. 96, 2993-3009, 1994.

[13] This map is a composite of Field Sheet 1200097 from the Canadian Hydrographic Service (April-May 1994) with data from Field Sheet 3499 of the Defence Research Establishment Pacific (Survey 1993/94).

[14] Heard, G.J., McDonald M, Chapman, N.R., Jaschke, L. Underwater light bulb implosions: A useful acoustic source. IEEE Oceans 97 conference proc. Vol III. October 6-9 Halifax, pp 755-762. 1997.

[15] Porter, M. The KRAKEN normal mode program, SACLANTCEN Memorandum 245, 1991.

[16] Jensen F.B., W.A. Kuperman, M.B. Porter, H. Schmidt, *Computational Ocean Acoustics*, AIP Press, New York, 1994.

[17] W. H. Press, S. A. Teukolsky, W. T. Vetterling, and B. P. Flannery, *Numerical Recipes in FORTRAN*, 2nd ed. (Cambridge University Press, Cambridge, 1992), Chap. 10, 1992.

[18] S. E. Dosso, M. J. Wilmut, and A. S. Lapinski, "An adaptive-hybrid algorithm for geoacoustic inversion," IEEE J. Ocean Eng. 26, 324-336, 2001.

[19] Brooke, G.H., D.J. Thomson, G.R. Ebbeson, PECan: a Canadian parabolic equation model for underwater sound propagation, J. of Comp. Acoust., 9(1), pp. 69-100, 2001.

[20] Schmidt, H. SAFARI – Seismo-acoustic fast field algorithm for range independent environments, User's guide, SACLANTCEN Report 113, 1988.